Comparison of Ni based and Rh based catalysts performance in the oxidative steam reforming of raw bio-oil

Aingeru Remiro*, Aitor Arandia, Javier Bilbao, Ana G. Gayubo

Chemical Engineering Department, University of the Basque Country, P. O. Box 644, 48080. Bilbao, Spain. Phone: +34 946 015361. Fax: +34 946 013 500

**email: aingeru.remiro@ehu.es*

Abstract

The effect of O_2 content in the oxidative steam reforming (OSR) of raw bio-oil has been studied, and the kinetic behavior, particularly deactivation, has been compared between two catalyst (Ni/La_2O_3-αAl_2O_3 and Rh/CeO_2-ZrO_2). The experiments have been carried out in an equipment with two steps in series: 1) thermal treatment (at 500 ºC, for the controlled deposition of pyrolytic lignin), and; 2) catalytic *in-line* reforming in a fluidized bed. The reaction conditions have been as follows: oxygen/carbon ratio (O/C), 0, 0.17, 0.34 and 0.67; 700 ºC; steam/carbon ratio (S/C), 6; space time, 0.3 $g_{catalyst}h/g_{bio\text{-}oil}$ (for Ni/La_2O_3-αAl_2O_3) and 0.15 $g_{catalyst}h/g_{bio\text{-}oil}$ (for Rh/CeO_2-ZrO_2); time on stream, 4 h. The content and morphology of the coke deposited on the catalysts has been determined by temperature programmed oxidation (TPO), and the deterioration of the metallic properties of the catalysts by temperature programmed reduction (TPR) and X-ray diffraction (XRD).

The results (bio-oil conversion, products yield and their evolution with time on stream) show that for Rh/CeO_2-ZrO_2 catalyst the decrease in coke deposition as O/C ratio is increased involves attenuation of catalyst deactivation. Consequently, this catalyst is stable after 24 h operation for high O/C ratios, thus keeping constant the activity for reforming reactions and the WGS reaction, with a high yield of H_2 and low yields of CO, CH_4 and hydrocarbons. However, for the Ni/La_2O_3-αAl_2O_3 catalyst of lower activity than the Rh/CeO_2-ZrO_2, the

decrease in coke content as O/C ratio is increased does not involve a noticeable attenuation in catalyst deactivation, which is due to Ni sintering.

Keywords: bio-oil, oxidative steam reforming, steam reforming, hydrogen production, coke.

1. Introduction

The technological development of sustainable H_2 production routes from sources alternative to oil, particular from biomass, has a great interest in order to meet the increasing energy demand, thus avoiding the negative environmental impact of current technologies.[1,2] Steam reforming (SR) of bio-oil is an encouraging route for this objective, given that bio-oil can be obtained from lignocellulosic biomass in decentralized fast pyrolysis plants, with high yield and by means of simple and environmentally friendly technologies.[3,4] Moreover, the high water content in the bio-oil (above 35 wt %) is not an inconvenient for SR, whose global stoichiometry (by incorporating water gas shift (WGS) reaction) is:

$$C_nH_mO_k + (2n-k)H_2O \rightarrow nCO_2 + (2n+m/2-k)H_2 \quad (1)$$

Nevertheless, the industrial implementation of this process is limited by its endothermic nature and the requirement of energy supply. This energy requirement is avoided in the oxidative steam reforming (OSR) by co-feeding O_2 with the bio-oil.[5-8] Moreover, this strategy hinders CO production by CO oxidation reaction, which is highly desired for fuel cell systems.[2] The stoichiometry of the OSR reaction for bio-oil is:

$$C_nH_mO_k + pO_2 + (2n-k-2p)H_2O \rightarrow nCO_2 + (2n+m/2-k-2p)H_2 \quad (2)$$

Furthermore, with an appropriate O/S(steam)/C ratio in the OSR reaction, autothermal reforming (ATR) regime is achieved, which is suitable in small reforming units when there are energy supply limitations.[9]

It should also be noted that H_2 yield is lower than that corresponding to eq 2 stoichiometry, due to secondary reactions (decomposition/cracking of oxygenates in the bio-oil), in which by-product (CO, CH_4 and light hydrocarbons) are formed,[10] with their distribution depending on the reforming conditions.

The study of different alternatives for the reforming of raw bio-oil has been conditioned by the re-polymerization of phenolic compounds in the bio-oil derived from lignin pyrolysis,[11,12] with a carbonaceous material (pyrolytic lignin) being formed, which deactivates the catalyst and even hinders the flow through the reactor.[13-15] Different authors have proven that co-feeding O_2 with the bio-oil attenuates coke formation, and therefore catalyst deactivation, by the partial combustion of coke components.[16-18]

Furthermore, in spite of the aforementioned advantage of co-feeding O_2 to avoid energy supply and attenuate catalyst deactivation, this strategy has the inconvenient of lower H_2 yield and selectivity compared to the SR process due to the partial combustion of H_2, oxygenates in the bio-oil (mainly alcohols), and by-products (CH_4 and hydrocarbons).[9,19,20] Furthermore, Rioche et al.[21] found that, although coke deposition was noticeably attenuated in the presence of O_2, the deactivation of a $Pt/CeZrO_2$ catalyst was faster for a high O/C ratio due to Pt sintering.

This work explores the capacity of Ni and Rh catalysts (Ni/La_2O_3-αAl_2O_3 and Rh/CeO_2-ZrO_2) for the OSR of raw bio-oil, and pays especial attention to their deactivations (by coking and change in metal properties). Thus, a study has been carried out of the role paid by co-feeding O_2 (O/C ratio) in the content and nature of the coke and in the metal properties and evolution of product distribution with time on stream. Both catalysts have been selected because of their excellent behavior (activity, H_2 selectivity and stability) in the SR of ethanol and bio-oil.[22-26] The responsible for this behavior are the high activity for reforming of both metals (more active Rh, which is also more expensive) and the suitable composition of the suports.[27] Thus, the supports of La_2O_3-αAl_2O_3 and CeO_2-ZrO_2 for Ni and Rh catalysts, respectively, have a high capacity for adsorbing H_2O and storing oxygen, and therefore are active in the gasification and combustion of coke precursors.[26,28-30].

The catalysts have been used in a reaction system with two steps in line, which allows

minimizing the deactivation by pyrolytic lignin deposition. Accordingly, the pyrolytic lignin is deposited in a controlled way in the first step, and the remaining volatile compounds are reformed in the second step (catalytic reactor).[10] The co-feeding of O_2 into the system, which is characteristic of the OSR process, is a novelty over the previous studies in which the SR of raw bio-oil has been studied in this reaction system.[10,24-26]

2. Experimental

2.1. Catalysts

The Ni/La_2O_3-αAl_2O_3 catalyst (denoted as Ni/LaAl) was prepared with 10 wt % Ni and 9 wt % La, and calcined at 550 ºC, by using a previously described method.[26] The Rh/CeO_2-ZrO_2 catalyst (denoted as Rh/ZDC) was supplied by *Fuel Cell Materials*, with 2 wt % Rh content.

The catalysts have been characterized by: adsorption-desorption of N_2 in an *Autosorb iQ2* equipment from *Quantachrome* for calculating the BET specific surface area, pore volume and mean pore diameter; H_2 chemisorption, in the same equipment for determining dispersion and metal surface area; Temperature Programmed Reduction (TPR) in a *Micromeritics AutoChem 2920* for determining the reducibility of the metal species; X ray diffraction (XRD) in a *Bruker D8 Advance* difractometer for determining the different crystal phases present in the material.

The amount and nature of coke deposited on both catalysts has been determined by Temperature Programmed Oxidation (TPO) in a *TA Instrument SDT 2960* thermobalance.

2.2. Bio-oil production and composition

The raw bio-oil (whose properties are set out in Table 1) was obtained by flash pyrolysis of pine sawdust at 480 ºC, in a semi-industrial demonstration plant (Ikerlan-IK4 technology center, Alava, Spain), with a biomass feeding capacity of 25 kg/h.[31] The development of this

plant was based on previous results obtained in a laboratory plant (120 g/h) at the University of the Basque Country.[32,33] The water content in Table 1 was determined by Karl Fischer valorisation (*KF Titrino Plus 870*). The pH was measured with a Hanna Instruments pH meter model 8417, and the viscosity measurement was conducted using an Ubbelohde micro-viscosimeter with suspended level bulb at 40 ºC. The density was measured by picnometry at 40 ºC and the suspended solids content was determined by filtering the sample, previously diluted with acetone, at room temperature on a filter paper in a Buchner funnel equipped with a water suction pump, and by weighting the cake dried at 105 ºC.

The elemental analysis was obtained in a *Leco CHN-932 analyzer* and ultra-microbalance *Sartorious M2P*. The ash content was obtained after combustion in a *TA Instrument SDT 2960* thermobalance at 800 ºC and the high heating value of bio-oil was evaluated from its elemental composition (on a dry basis) with Dulong equation.[34]

The raw bio-oil composition (Table 2, on a water-free basis) was determined by GC/MS analyzer (*Shimadzu QP2010S device*).

Table 1

Table 2

2.3. Reaction equipment and operating conditions

Runs have been performed in an automated reaction equipment (*MicroActivity Reference* from *PID Eng&Tech*, Figure 1) provided with two units in series (thermal step and catalytic step) of stainless steel.[10] The thermal step consists of a U-shaped tube at 500 ºC for repolymerization of the oxygenates derived from lignin pyrolysis. In this step, 11 wt % of the raw bio-oil oxygenate content was deposited (as pyrolytic lignin) and the corresponding molecular formula of the bio-oil exiting this step is $C_{3.8}H_{7.7}O_{2.9}$ (water-free basis), which has

been determined by elemental balances to C, H and O. In the second unit (catalytic reforming reactor in fluidized bed regime), the catalyst is mixed with inert solid (SiC) (inert/catalyst mass ratio > 8/1) in order to ensure a correct fluidization regime. It should be noted that the uniformity of properties in the fluidized bed guarantees bed isothermicity and also representativeness in the results for the analysis of the deactivated catalyst.

Prior to each kinetic run, the catalyst is reduced in H_2-N_2 stream (10 vol % de H_2) at 700 ºC for 2 h. The kinetic runs have been carried out at atmospheric pressure, with the remaining operating conditions being as follows: 700 ºC (required for avoiding an excessively fast deactivation without co-feeding O_2);[25] steam/carbon (S/C) molar ratio in the feed, 6, which is obtained by co-feeding water (*307 Gilson pump*) with the raw bio-oil (*injection pump Harvard Apparatus 22*); oxygen/carbon ratios (O/C), 0, 0.17, 0.34, and 0.67 (the last one corresponding to autothermal regime); space time, 0.3 $g_{catalyst}h/g_{bio\text{-}oil}$ for Ni/LaAl catalyst, and 0.15 $g_{catalyst}h/g_{bio\text{-}oil}$ for Rh/ZDC catalyst (these values have been established based on previous experiments and are different for the two catalysts studied due to the higher activity of the Rh/ZDC catalyst).

Figure 1

The products stream is analyzed in-line with a *MicroGC 490* from *Agilent*, equipped with 4 analytic channels: molecular sieve MS5 for quantifying H_2, N_2, O_2, CH_4 and CO; Plot Q for CO_2, H_2O and C_2-C_4 hydrocarbons; CPSIL for C_5-C_{11} hydrocarbons, and; Stabilwax for oxygenated compounds.

2.4. Reaction indices

The following reaction indices have been used for quantifying the kinetic behavior:

Bio-oil conversion: $$X_{bio\text{-}oil} = \frac{F_{in} - F_{out}}{F_{in}} \quad (3)$$

where F_{in} and F_{out} are the molar flow rate of bio-oil at the reactor inlet and outlet, respectively, in C units contained.

H_2 yield: $$Y_{H_2} = \frac{F_{H_2}}{F^{o}_{H_2}} \quad (4)$$

where F_{H2} is the H_2 molar flow rate in the product stream and F^0_{H2} is the stoichiometric molar flow rate (by C units of the bio-oil fed into the reforming reactor), which has been evaluated for the SR reaction as $(2n+m/2-k)\cdot F_{in}$, according to eq 3.

The yield of carbon-containing products (CO_2, CO, CH_4 and light hydrocarbons):

$$Y_i = \frac{F_i}{F_{in}} \quad (5)$$

where F_i is the molar flow rate of each compound (in C equivalent units).

The flow rates in eqs 3-5 have been determined by C balances with the inlet stream being the bio-oil at the reactor inlet (0.08 ml/min) and the outlet stream the reaction products (quantified by chromatograph) and taking into account the amount of pyrolitic lignin deposited in the thermal unit. Accordingly, a balance closure above 95 wt% is attained, with the relative error (based on replicates) being lower than 4 %.

3. Results and Discussion

3.1. Catalysts' properties

The physical properties (BET surface area, pore volume and mean pore diameter) and metallic properties (dispersion and metal surface area) are set out in Table 3. It must be pointed out that BET surface area of Rh/ZDC catalyst (85.7 m^2/g) is double that of Ni/LaAl

catalyst, and its metal dispersion (72.4 %) is more than ten times higher, due to the low Rh content, which favors the formation of highly dispersed nanoparticles on the support surface.[35]

Table 3

Figure 2 shows the TPR profiles of both catalysts. The TPR profile for Ni/LaAl catalyst calcined at 550 ºC reveals that different metal phases are reduced within specific temperature ranges, according to the following sequence:[36-38] i) the peaks below 350 °C correspond to the reduction of bulk NiO clusters with low interaction with the support; ii) the main reduction band, in the 350-700 °C range, has been ascribed to the reduction of dispersed NiO_x species, which are probably amorphous and interact strongly with the support; iii) the reduction above 700 °C corresponds to the $NiAl_2O_4$ spinel, which has been probably formed by migration of Ni atoms on Al_2O_3.[39] The position of the reduction band in the 350-700 °C range depends on the phase of Al_2O_3, so that it appears at lower temperatures for Ni/La_2O_3/γ-Al_2O_3 catalyst than for Ni/La_2O_3/α-Al_2O_3.[40] The two reduction peaks located at different temperatures in this range have been attributed in literature to the reduction of NiO species interacting differently with the support.[38] Thus, Mazunder and de Lasa[41] identified two reduction peaks at approximately 500 ºC and 600 °C, which were attributed to two types of surface spinels formed by accommodating Ni ions in the octahedral and tetrahedral sites of Al_2O_3, respectively. Nevertheless, for a Ni/γ-Al_2O_3 catalyst modified with 10 wt % La, Sugisawa et al.[42] attributed the presence of the highest peak at approximately 520 °C to the reduction of $LaNiO_3$.

For Rh/ZDC catalyst a peak at 65 ºC is observed, which is ascribed to the reduction of Rh_2O_3 to Rh^0,[43] whereas the second peak, at around 200 ºC, is associated with the reduction of

surface CeO_2 species in the support, whose reduction is favored by the presence of Rh, due to the spillover phenomena.[44,45]

Figure 2

In the XRD diffractogram of non-reduced Ni/LaAl catalyst (Figure 3), the presence of NiO, ($NiAl_2O_4$) spinel, $LaAlO_3$ and Al_2O_3 species is observed. Subsequent to reduction (at 700 ºC), Ni^0 metallic sites (derived from NiO reduction) are observed at 2θ = 44.8 and 52°. Rh/ZDC catalyst contains a mixture of Ce and Zr oxides, and the presence of Rh_2O_3 prior to reduction, or Rh^0 after reduction is not observed, which is explained because of the low Rh content and its high dispersion on the support (Table 3).

Figure 3

3.2. Ni/LaAl catalyst performance

The effect of O/C ratio in the feed (0, 0.17, 0.34 and 0.67) on the evolution with time on stream of bio-oil conversion and products yield is shown in Figures 4 and 5, respectively, for Ni/LaAl catalyst. Figure 4a shows that the conversion of bio-oil oxygenates is complete at zero time on stream (fresh catalyst) for all the O/C ratios. Furthermore, the highest H_2 yield at zero time on stream (around 0.9) is obtained for O/C = 0 (Figure 4b), and under these conditions the yields of CH_4 (Figure 5c) and light hydrocarbons (Figure 5d) are insignificant. As the O/C ratio is increased, the yields of H_2 (Figure 4b) and CO (Figure 5b) at zero time on stream decrease and that of CO_2 increases (Figure 5a), because the combustion of the former is favored.

Figure 4

Figure 5

As time on stream is increased, the yields of H_2 (Figure 4b) and CO_2 (Figure 5a) decrease and the yield of CO increases (Figure 5b), due to the loss of activity for water gas shift (WGS) reaction. The yields of CH_4 (Figure 5c) and hydrocarbons (Figure 5d) increase because their reforming reaction rate decreases. Moreover, it should be noted that, due to the undesired catalyst deactivation, there is an increase in the reaction rate of the thermal routes (decomposition of bio-oil oxygenates, with formation of CO_2, CO, CH_4 and hydrocarbons, and oxidation of all products, except CO_2), which contribute to the results in Figures 4 and 5. These thermal reactions take place in parallel with the catalytic ones (reforming of oxygenates and by-products, WGS reaction, and catalytic oxidation of reaction medium compounds), and their significance is enhanced by catalyst deactivation.

Concerning the effect of O/C ratio on the evolution with time on stream of reaction indices, it is observed that an increase in this ratio attenuates the rate of decrease in bio-oil oxygenates conversion (Figure 4a), but does not attenuate the decreasing trend in H_2 yield, which decreases to a constant value (around 0.1 for 3 h time on stream) for all the O/C ratios studied (Figure 4b). Furthermore, the yield of CO_2 decreases with time on stream to a stable value (Figure 5a). The fact that this value is higher as O/C ratio is increased may be attributed to the enhancement of bio-oil oxygenates combustion. This result is consistent with those for bio-oil conversion (Figure 4a), which keeps constant for 4h time on stream for O/C = 0.67. In addition to the partial combustion of bio-oil oxygenates under severe deactivation conditions, an increase in O/C ratio also favors slightly H_2 combustion (Figure 4b) and considerably hydrocarbon combustion (Figure 5d). Nevertheless, the combustion of CH_4 is not favored by increasing O/C ratio (Figure 5c).

The aforementioned results in Figures 4b and 5 are evidence that, under the reaction conditions studied (700 ºC), an increase in the O/C ratio does not imply a significant attenuation in the catalyst deactivation for reforming or WGS reactions, given that the rate of

change in product yields is hardly affected by the O/C ratio. In order to explain these results, the deactivated catalysts have been characterized by analyzing both the coke deposited (TPO profiles) and the changes produced in the metal structure (TPR and XRD profiles). Accordingly, the relative significance is identified for the deactivation by coke deposition and by other possible causes related to Ni sites (oxidation and/or sintering).

Figure 6a shows the TPO profiles corresponding to the combustion of the coke deposited on Ni/LaAl catalyst deactivated in the runs of Figures 4 and 5. Figure 6b shows the effect of the O/C ratio on the total coke content (calculated from the area under the TPO curve). Two different peaks are clearly identified and, based on their assignment in the deactivation of Ni catalysts used in the reforming of ethanol and bio-oil,[10,46-48] they correspond to the combustion of coke fractions of different nature deposited in different locations on the spent catalyst: i) the fraction that burns at lower temperature (at around 415 ºC) corresponds to the encapsulating coke deposited on metal sites, whose combustion is activated by these sites, and; ii) the fraction that burns at higher temperature (600 ºC), corresponds to the coke deposited on the catalyst support. The formation of these two coke types occurs according to two different mechanisms, although synergy may also be possible. The coke that blocks Ni sites (encapsulating) is of amorphous nature and its formation is attributed mainly to the repolymerization of phenolic compounds in the bio-oil,[49] apart from the decomposition of other unstable compounds in the bio-oil. Given the origin of this type of coke, its formation is very fast. The coke that burns at higher temperatures, and whose combustion is not activated by the direct contact with the metal sites, is a structured coke containing a significant amount of condensed polyaromatics, whose formation mechanism is related to the decomposition of CH_4 and by-product hydrocarbons. The C atoms generated lead to intermediate compounds on the Ni particles, which condense forming ordered structures separated from Ni sites, with their configurations being fibers or nanotubes.[50-52]

The results in Figure 6a show that for O/C = 0.17 there is no decrease in any coke fraction deposited on the catalyst compared to SR conditions (O/C = 0), which is evidence that for this low concentration of O_2 only reaction medium gases are burnt. This combustion affects mainly the yields of H_2 and CO, which notably decrease (Figures 4b and 5b). Nevertheless, for O/C = 0.34, the O_2 concentration in the reaction medium is enough for partial combustion of the intermediates in the mechanism of coke formation, and therefore coke content decreases from 9.5 wt %, for a feed without O_2, to 3.0 wt %, for O/C = 0.34 (Figure 6b). The increase in O/C ratio from 0.34 to 0.67 contributes to a further attenuation of coke deposition. Furthermore, the increase in O/C ratio affects similarly to both types of cokes identified (Figure 6a), and therefore the combustion of precursors and intermediate compounds is enhanced throughout the formation of both types of cokes.

Figure 6

The comparison of the effect of O/C ratio on the results of coke content deposited on Ni/LaAl catalyst (Figure 6) with those corresponding to the evolution with time on stream of reaction indices (Figures 4b and 5) shows that there is only a small attenuation of Ni/LaAl catalyst deactivation for reforming reactions and WGS, which is not consistent with the noticeable decrease in coke content as O/C ratio is increased. This inconsistency should be attributed to the existence of other causes of deactivation, which mask the effect of coke deposition on catalyst deactivation. The possible Ni oxidation due to the presence of O_2 in the reaction medium has been discarded by TPR and XRD analysis of the catalyst deactivated under SR and OSR conditions. Thus, no reduction peak has been observed in the TPR profiles (not shown), which is evidence of the absence of oxidized Ni species. Similarly, the XRD diffractograms (Figure 7) show the absence of diffraction peaks at 2θ = 43.3 º (2 0 0) and 62.9 º (2 2 0) corresponding to NiO. Nevertheless, the results of this analysis show that the average Ni particle size of the catalysts deactivated under SR conditions (O/C = 0) (12.5 nm,

determined by means of Scherrer equation from the width of the peak at 2θ = 52 º corresponding to Ni^0 in the (2 0 0) plane) is noticeably higher than that of the fresh catalyst (7 nm). The Ni particle size in the catalyst deactivated under OSR conditions (O/C = 0.67), (12.6 nm) is very similar to that deactivated under SR conditions. This result evidences that Ni sintering is an important cause of deactivation at this high reforming temperature, which masks the contribution of coke deposition to deactivation under these conditions, and explains the small attenuation in catalyst deactivation by increasing O/C ratio.

Figure 7

3.3. Rh/ZDC catalyst performance

Figures 8 and 9 show the effect of O/C ratio on the evolution with time on stream of bio-oil conversion (Figure 8a) and the yields of H_2 (Figure 8b) and the remaining products (Figure 9), in the OSR of raw bio-oil with Rh/ZDC catalyst. It should be noted that these experiments have been carried out with the same temperature (700 ºC) and S/C ratio (6) than those mentioned in section 3.2 for Ni/LaAl catalyst.

Firstly, it is observed that Rh/ZDC catalyst is more active than Ni/LaAl catalyst for SR reactions. Thus, although space time is half (0.15 and 0.30 $g_{catalyst}h/g_{bio\text{-}oil}$ for Rh/ZDC and Ni/LaAl catalysts, respectively), total bio-oil conversion is obtained up to 0.5 h time on stream for all the studied O/C ratios (Figure 8a), and the H_2 yield at zero time on stream for Rh/ZDC catalyst is 0.96 without O_2 in the feed (Figure 8b), which is slightly higher than the value (0.89) obtained with Ni/LaAl catalyst (Figure 4b). Moreover, the yields of CO_2 (Figure 9a) and CO (Figure 9b) are higher and lower, respectively, than those obtained with Ni/LaAl catalyst, which indicates that Rh/ZDC catalyst is also more active for WGS reaction. Moreover, at zero time on stream, the increase in O/C ratio has a qualitatively similar effect as that observed for Ni/LaAl catalyst (Figure 5), thus decreasing the yields of H_2 (Figure 8b) and

CO (Figure 9b) and increasing the yield of CO_2 (Figure 9a) due to the partial combustion of the former and oxygenates.

Concerning the deactivation of the catalyst, Figures 8 and 9 show that, differently to the results for Ni/LaAl catalyst, the O/C ratio significantly affects the evolution with time on stream of both conversion and product yields. Under SR conditions (O/C = 0), the conversion slightly decreases between 0.5 and 3 h time on stream, and subsequently the decrease is noticeable. The increase in the O/C ratio favors constant conversion (Figure 8a), with this being almost full along 4 h time on stream for O/C = 0.67. Similarly, the increase in O/C ratio favors almost constant H_2 yield. Thus, for O/C = 0.67, subsequent to an initial decrease between 0.5-1 h, the H_2 yield keeps stable at a value of 0.45 above 1 h time on stream (Figure 8b). It should be noted that the H_2 yield evolution with time on stream shown in Figure 8b for different O/C ratios has a general trend related to the successive periods and catalyst states, i.e., thermodynamic regime, deactivation and pseudo-stability of the catalyst. The duration of the first period, in which there is catalyst excess, is approximately 45 min for O/C = 0 and this duration decreases by increasing O/C ratio, being 0.5 h for O/C = 0.67. Furthermore, the deactivation rate in the second period decreases with O/C ratio, and for O/C = 0.67 an stable state is achieved after 1 h time on stream, in which H_2 yield remains constant at around 0.45. In this state, coke formation rates balance the rates for its combustion and gasification.

Moreover, the trend of the effect of O/C ratio on the evolution with time on stream of CO_2 yield (Figure 9a) is similar to the aforementioned trend for H_2 yield, which evidences that an increase in O/C ratio is efficient for improving catalyst stability, and therefore attenuating the activity decrease for reforming, WGS and oxidation reactions. Consequently, the increase in CO yield with time on stream is less pronounced, and for O/C = 0.67 this yield keeps constant (Figure 9b).

Furthermore, the evolution with time on stream of the yield of CH_4 (Figure 9c) and hydrocarbons (Figure 9d) shows that the initial deactivation selectively affects the reforming of these compounds, whose yield increases with time on stream. An increase in O/C ratio does not affect significantly the evolution with time on stream of CH_4, but it is efficient for attenuating the increase in hydrocarbons yield, whose value remains constant with time on stream for a O/C ratio of 0.67 (Figure 9d).

Figure 8

Figure 9

In order to explain the aforementioned results of the effect O/C ratio on Rh/ZDC catalyst deactivation, the deactivated catalyst have been analyzed by means of TPO (in order to determine the amount and nature of the coke deposited) and TPR (in order to determine the oxidation state of metal particles in the deactivated catalyst).

Figure 10a shows the TPO profiles for coke combustion corresponding to the catalyst used in the experiments in Figures 8 and 9. Two coke fractions are distinguished, which burn at lower temperature than the coke fractions deposited on Ni/LaAl catalyst (Figure 6). These differences in the TPO profiles are related to the higher activity of Rh than Ni for coke combustion. Moreover, the excellent redox properties of CeO_2 in the support are well-known, as well as its capacity for O_2 storage,[53-57] which enhances lattice oxygen exchange with O_2 in the gas phase and favors coke combustion.[58] Thus, the first peak, presumably corresponding to the coke deposited on Rh metal sites (encapsulating coke), has a maximum at 300 ºC, whereas the second peak (coke deposited on the support) has its maximum at around 410 ºC. Furthermore, under SR conditions a shoulder is observed at 325 ºC, which suggests the existence of another coke fraction, deposited near the metal-support interphase,[46] whose combustion is favored by the proximity of the metal.

Figure 10

Likewise, as observed in Figure 10b, total coke content decreases by increasing O/C ratio, which affects selectively the coke fraction that burns at low temperature for moderate O/C ratios (0.17 and 0.34) (first peak in Figure 10a). As O/C ratio is increased, the first combustion peak shifts towards lower temperatures and the shoulder at intermediate temperature disappears, which evidences that the presence of O_2 in the reaction medium notably modifies coke composition. This observation is coherent with the results obtained using MALDI-TOF MS (matrix assisted laser desorption/ionization time-of-flight mass spectrometry) by Lemonidou et al.[58], who attributed the ability to avoid oligomerization and condensation reactions involving coke precursors to the O_2 in the reaction medium, which leads to a coke with low molecular weight species, which are more reactive and easily burned.

Furthermore, the fact that the coke fraction that burns at high temperature does not decrease by co-feeding O_2, except for a very high O/C ratio (O/C = 0.67) (Figure 10a), evidences that this coke fraction (presumably deposited on the support) is not responsible for catalyst deactivation. Thus, a comparison of the results of coke content attenuation when O/C ratio is increased (Figure 10) with the afore-mentioned results of attenuation of deactivation (Figures 8 and 9) allows concluding that the deactivation should be attributed to the encapsulating coke fraction deposited on Rh, whose combustion takes place at low temperature (at around 300 ºC) (first peak in Figure 10a).

Figure 11 shows the TPR profiles for the Rh/ZDC catalyst deactivated under SR conditions (O/C = 0) and OSR conditions (O/C = 0.67). As observed, both TPR profiles show the presence of a reduction peak below 100 ºC, which is evidence that certain Rh metal sites have been partially oxidized during the reaction. Based on the results, this change in the oxidation state of Rh is slightly more significant under OSR conditions. This oxidation of Rh particles

explains the decrease in catalyst activity above 30-45 min time on stream (depending on the O/C ratio) in Figures 8 and 9.

Figure 11

3.4. Comparison of catalysts and stability of the Rh/ZDC catalyst

The aforementioned results are evidence of the high activity of the catalysts studied for the SR of raw bio-oil, so that conversion is full at zero time on stream, and H_2 yields of up to 0.89 and 0.96 are attained for Ni/LaAl and Rh/ZDC catalysts, respectively. Moreover, the lower CO yield is obtained with Rh/ZDC, which evidences the higher activity of this catalyst than Ni/LaAl, for the WGS reaction. This result is consistent with the well-known activity of CeO_2 for the WGS reaction.[45]

Deactivation by coking attenuates as O_2 is co-fed, but this leads to a different behavior of the two catalysts in the OSR reaction. The previously shown TPO profiles (Figures 6 and 10) show the heterogeneity of the coke deposited in both catalysts, which is made up of two fractions, with deactivation being mainly caused by the encapsulating coke fraction that blocks the metal active sites, whose combustion is selectively favored by increasing the O/C ratio in the case of the spent Rh/ZDC catalyst. The TPO profiles also reveal that the presence of O_2 in the reaction medium involves a significant decrease in coke deposition on both catalysts, with contents being of around 1 wt % for O/C = 0.67 (autothermal regime).

Nevertheless, the comparison of deactivation rate for both catalysts (Figures 4b and 5 for Ni/LaAl and Figures 8 and 9 for Rh/ZDC) shows that the decrease in coke content only has a favorable effect on attenuating deactivation of Rh/ZDC catalyst. For this catalyst, a first deactivation period occurs, which is due to the partial oxidation of Rh metal particles. Subsequently, catalyst deactivation takes place by coke deposition, and under OSR conditions the Rh/ZDC catalyst attains a pseudo-stable state in which coke deposition is avoided by the

combustion of the forming intermediates, and therefore the catalyst keeps a constant activity for reforming and WGS reactions.

Rh/ZDC catalyst has been proven to be stable at 700 ºC and under OSR conditions (O/C = 0.34) for 24 h time on stream runs for a high space time (0.6 $g_{catalyst}h/g_{bio-oil}$, Figure 12). The results show that, subsequent to an initial period of deactivation, bio-oil conversion and the yields of H_2, CO_2, CO, CH_4 and hydrocarbons keep constant with time on stream. A comparison of Figures 8 and 9 with Figure 12 reveals that the duration of the pseudo-stable period depends on the reaction conditions. Thus, for a low space time of 0.15 $g_{catalyst}h/g_{bio-oil}$ and a O/C ratio of 0.67 (corresponding to the autothermal regime) a constant H_2 yield of 0.45 is obtained for 4 h time on stream (Figure 8b), whereas for a high space time, 0.60 $g_{catalyst}h/g_{bio-oil}$; and a O/C ratio of 0.34 a constant H_2 yield of 0.57 is obtained for 24 h time on stream (Figure 12).

Figure 12

Furthermore, in view of the high activity of the Rh/ZDC catalyst for coke combustion (due to the activity of Rh and CeO_2-ZrO_2 support for combustion), it is an interesting option for fast regeneration and use at larger scale in successive reaction-regeneration cycles.

The apparent inconsistency regarding Ni/LaAl catalyst, for which an increase in O/C ratio attenuates coke deposition without attenuation in the deactivation of reforming and WGS reactions, is explained by Ni sintering under these reaction conditions (700 ºC), which has been proven by XRD analysis.

4. Conclusions

It has been proven that a commercial catalyst of Rh supported on CeO_2-ZrO_2 is suitable for up-grading bio-oil by OSR. The main cause of catalyst deactivation for reforming and WGS

reactions is the deposition of encapsulating coke that blocks Rh sites, but the presence of O_2 in the reaction medium contributes to decreasing this deposition of encapsulating coke and attenuating deactivation. Furthermore, a slight change occurs in Rh oxidation state, which contributes to a slight deactivation of the catalyst. Consequently, subsequent to a small decrease in activity for a short time on stream under OSR conditions, Rh/ZDC catalyst attains a stable performance and the yield of H_2 keeps constant for a period of time depending on the reaction conditions. Thus, for 0.60 $g_{catalyst}h/g_{bio\text{-}oil}$ and a O/C ratio of 0.34 a constant H_2 yield of 0.57 is obtained for 24 h time on stream. The redox properties of CeO_2-ZrO_2 support favour the combustion of coke precursors and allow the catalyst achieving a pseudo-stable state in which coke deposition rate on metal sites equals its removal by combustion. Accordingly, this catalyst and reaction conditions allow keeping the yield of by-products, CO, light hydrocarbons and methane with time on stream in a constant rather low value.

Nevertheless, the La_2O_3-αAl_2O_3 supported Ni catalyst, less active than Rh, is not stable for raw bio-oil OSR, although the presence of O_2 in the reaction medium also attenuates coke deposition, because the sintering of metal particles is an important cause of deactivation at the high temperature (700 ºC) required for attaining high bio-oil conversion. For this catalyst, H_2 yield decreases with time on stream to low values (of around 0.10 subsequent to 4 h time on stream) and the yield of by-products increases.

Acknowledgements

This work was carried out with the financial support of the Department of Education Universities and Investigation of the Basque Government (IT748-13), the University of the Basque Country (UFI 11/39 and Remiro's Postdoctoral grant) and the Ministry of Economy and Competitiveness of the Spanish Government jointly with the European Regional

Development Funds (AEI/FEDER, UE) (Projects CTQ2012-35263 and CTQ2015-68883-R and Ph.D. grant BES-2013-063639 for A. Arandia).

Nomenclature

C_c coke content, wt %

d_p mean pore diameter, nm

HHV high heating value, MJ Kg^{-1}

F_{in}, F_{out} molar flow rate of bio-oil at the reactor inlet and outlet, respectively, in C content units, mol h^{-1}

F_i molar flow rate of i carbon containing product at the reactor outlet, in C content units, mol h^{-1}

F_{H2} molar flow rate of H_2 at the reactor outlet, mol h^{-1}

F^o_{H2} stoichiometric molar flow rate of H_2 at the reactor outlet, for SR, mol h^{-1}

O/C oxygen-to-carbon ratio

S/C steam-to-carbon ratio

S_{BET} BET surface, m^2 g^{-1}

S_m metal surface area, m^2 g_{metal}^{-1}

V_p pore volume, cm^3 g^{-1}

$X_{bio\text{-}oil}$ conversion of bio-oil

Y_{H2} hydrogen yield

Y_i yield of *i* carbon containing product (CO, CO_2, CH_4, C_2-C_4)

References

(1) Li, D.; Li, X.; Gong, J. *Chem. Rev.* **2016**, *116*, 11529–11613.

(2) Navarro, R.M.; Peña, M.A.; Fierro, J.L.G. *Chem. Rev.* **2007**, *107*, 3952–3991.

(3) Mei, Y.; Wu, C.; Liu, R. *Int. J. Hydrogen Energy* **2016**, *41*, 9145–9152.

(4) Xie, H.; Yu, Q.; Zuo, Z.; Han, Z.; Yao, X.; Qin, Q. *Int. J. Hydrogen Energy* **2016**, *41*, 2345–2353.

(5) Geissler, K.; Newson, E.; Vogel, F.; Truong, T.B.; Hottinger, P.; Wokaun, A. *Phys. Chem. Chem. Phys.* **2001**, *3*, 289–293.

(6) Schuessler, M.; Lamla, O.; Stefanovski, T.; Klein, C.; zur Megede, D. *Chem. Eng. Technol.* **2001**, *24*, 1141–1145.

(7) Mo, L.; Zheng, X.; Yeh, C.-T. *Chem. Commun.* **2004**, 1426–1427.

(8) Wan, A.; Yeh, C.-T. *Catal. Today* **2007**, *129*, 293–296.

(9) Czernik, S.; French, R. *Int. J. Hydrogen Energy* **2014**, *39*, 744–750.

(10) Remiro, A.; Valle, B.; Aguayo, A.T.; Bilbao, J.; Gayubo, A.G. *Energ. Fuels* **2013**, *27*, 7549–7559.

(11) Salehi, E.; Seyedeyn-Azad, F.; Harding, T.; Abedi, J. *Fuel Process. Technol.* **2011**, *92*, 2203–2210.

(12) Seyedeyn-Azad, F.; Abedi, J.; Harding, T. *Chem. Eng. J.* **2012**, *180*, 145–150.

(13) Garcia, L.; French, R.; Czernik, S.; Chornet, E. *Appl. Catal. A-Gen.* **2000**, *201*, 225–239.

(14) Valle, B.; Castaño, P.; Olazar, M.; Bilbao, J.; Gayubo, A.G. *J. Catal.* **2012**, *285*, 304–314.

(15) Remiro, A.; Valle, B.; Aramburu, B.; Aguayo, A.T.; Bilbao, J.; Gayubo, A.G. *Ind. Eng. Chem. Res.* **2013**, *52*, 17087–17098.

(16) Paasikallio, V.; Azhari, A.; Kihlman, J.; Simell, P.; Lehtonen, J. *Int. J. Hydrogen Energy* **2015**, *40*, 12088–12096.

(17) Rennard, D.; French, R.; Czernik, S.; Josephson, T.; Schmidt, L. *Int. J. Hydrogen Energy* **2010**, *35*, 4048–4059.

(18) Hu, X.; Lu, G. *Int. J. Hydrogen Energy* **2010**, *35*, 7169–7176.

(19) Gutierrez, A.; Karinen, R.; Airaksinen, S.; Kaila, R.; Krause, A. *Int. J. Hydrogen Energy* **2011**, *36*, 8967–8977.

(20) Harju, H.; Lehtonen, J.; Lefferts, L. *Catal. Today* **2015**, *244*, 47–57.

(21) Rioche, C.; Kulkarni, S.; Meunier, F.C.; Breen, J.P.; Burch, R. *Appl. Catal. B-Environ.* **2005**, *61*, 130–139.

(22) Vicente, J.; Ereña, J.; Olazar, M.; Benito, P.L.; Bilbao, J.; Gayubo, A.G. *J. Energy Chem*. **2014**, *23*, 639–644.

(23) Gayubo A.G.; Vicente, J.; Ereña, J.; Montero, C.; Olazar, M.; Bilbao, J. *Catal. Lett.* **2014**, *144*, 1134–1143.

(24) Remiro, A.; Valle, B.; Oar-Arteta, L.; Aguayo, A.T.; Bilbao, J.; Gayubo, A.G. *Int. J. Hydrogen Energy* **2014**, *39*, 6889–6898.

(25) Remiro, A.; Valle, B.; Aguayo, A.T.; Bilbao, J.; Gayubo, A.G. *Fuel Process. Technol.* **2013**, *115*, 222–232.

(26) Valle, B.; Remiro, A.; Aguayo, A.T.; Bilbao, J.; Gayubo, A.G. *Int. J. Hydrogen Energy* **2013**, *38*, 1307–1318

(27) Mawdsley, J.R.; Krause, T.R. *Appl. Catal. A-Gen.* **2008**, *334*, 311–320.

(28) Malaibari, Z.O.; Amin, A.; Croiset, E.; Epling, W. *Int. J. Hydrogen Energy* **2014**, *39*, 10061–10073.

(29) Baruah, R.; Dixit, M.; Basarkar, P.; Parikh, D.; Bhargav, A. *Renew. Sust. Energ. Rev.* **2015**, *51*, 1345–1353.

(30) Mondal, T.; Pant, K.K.; Dalai, A.K. *Int. J. Hydrogen Energy* **2015**, *40*, 2529–2544.

(31) Fernández-Akarregi, A.R.; Makibar, J.; López, G.; Amutio, M.; Olazar, M. *Fuel Process. Technol.* **2013**, *112*, 48–56.

(32) Amutio, M.; Lopez, G.; Aguado, R.; Artetxe, M.; Bilbao, J.; Olazar, M. *Fuel* **2012**, *95*, 305–311.

(33) Amutio, M.; Lopez, G.; Aguado, R.; Bilbao, J.; Olazar, M. *Energ. Fuels* **2012**, *26*, 1353–1362.

(34) Scholze, B.; Meier, D. *J. Anal. Appl. Pyrol.* **2001**, *60*, 41–54.

(35) Li, Y.; Wang, X.; Song, C. *Catal. Today* **2016**, *263*, 22–34.

(36) Natesakhawat, S.; Watson, R.; Wang, X.; Ozkan, U. *J. Catal.* **2005**, *234*, 496–508.

(37) Valle, B.; Aramburu, B.; Remiro, A.; Bilbao, J.; Gayubo, A.G. *Appl. Catal. B-Environ.* **2014**, *147*, 402–410.

(38) Montero, C.; Remiro, A.; Arandia, A.; Benito, P.L.; Bilbao, J.; Gayubo, A.G. *Fuel Process. Technol.* **2016**, *152*, 215–222.

(39) Li, C.; Chen, Y. *Thermochim. Acta* **1995**, *256*, 457–465.

(40) Xu, J.; Zhou, W.; Wang, J.; Li, Z.; Ma, J. *Chinese J. Catal.* **2009**, *30*, 1076–1084.

(41) Mazumder, J.; de Lasa, H.I. *Appl. Catal. B-Environ.* **2015**, *168-169*, 250–265.

(42) Sugisawa, M.; Takanabe, K.; Harada, M.; Kubota, J.; Domen, K. *Fuel Process. Technol.* **2011**, *92*, 21–25.

(43) Eriksson, S.; Rojas, S.; Boutonnet, M.; Fierro, J.L.G. *Appl. Catal. A-Gen.* **2007**, *326*, 8–16.

(44) Rocchini, E.; Vicario, M.; Llorca, J.; Leitenburg, C.; Dolcetti, G.; Trovarelli, A. *J. Catal.* **2002**, *211*, 407–421.

(45) Oar-Arteta, L.; Remiro, A.; Epron, F.; Bion, N.; Aguayo, A.T.; Bilbao, J.; Gayubo, A.G. *Ind. Eng. Chem. Res.* **2016**, *55*, 3546–3555.

(46) Martin, N.; Viniegra, M.; Lima, E.; Espinosa, G. *Ind. Eng. Chem. Res.* **2004**, *43*, 1206–1210.

(47) Vicente, J.; Montero, C.; Ereña, J.; Azkoiti, M.J.; Bilbao, J.; Gayubo A.G. *Int. J. Hydrogen Energy* **2014**, *39*, 12586–12596.

(48) Montero, C.; Ochoa, A.; Castaño, P.; Bilbao, J.; Gayubo, A.G. *J. Catal.* **2015**, *331*, 181–192.

(49) Valle, B.; Aramburu, B.; Olazar, M.; Bilbao, J.; Gayubo, A.G. *Fuel*, **2017,** *submitted.*

(50) Karim, A.M.; Su, Y.; Sun, J.; Yang, C.; Strohm, J.J.; King, D.L.; Wang, Y. *Appl. Catal. B*, **2010**, *96*, 441–448.

(51) Helveg, S.; Sehested, J.; Rostrup-Nielsen, J.R. *Catal. Today*, **2011**, *178*, 42–46.

(52) Mahamulkar, S.; Yin, K.; Agrawal, P. K.; Davis, R. J.; Jones, C. W.; Malek, A.; Shibata, H. *Ind. Eng. Chem. Res.* **2016**, *55*, 9760-9818.

(53) Kugai, J.; Subramani, V.; Song, C.; Engelhard, M.H.; Chin, Y.-H. *J. Catal.* **2006**, *238*, 430–440.

(54) de Lima, S.M.; da Cruz, I.O.; Jacobs, G.; Davis, B.H.; Mattos, L.V.; Noronha, F.B. *J. Catal.* **2008**, *257*, 356–368.

(55) Pereira, E.B.; de la Piscina, P.R.; Marti, S.; Homs, N. *Energy Environ. Sci.* **2010**, *3*, 487–493.

(56) Pojanavaraphan, C.; Nakaranuwattana, W.; Luengnaruemitchai, A.; Gulari, E. *Chem. Eng. J.* **2014**, *240*, 99–108.

(57) Sedjame, H.J.; Fontaine, C.; Lafaye, G.; Barbier Jr, J. *Appl. Catal. B-Environ.* **2014**, *144*, 233–242.

(58) Lemonidou, A.A.; Vagia, E.C.; Lercher, J.A. *ACS Catal.* **2013**, *3*, 1919–1928.

Figure Captions

Figure 1. Scheme of the reaction equipment.

Figure 2. TPR profiles of the fresh catalysts.

Figure 3. XRD diffractograms of the fresh and fresh/reduced catalysts.

Figure 4. Effect of O/C ratio on the evolution with time on stream of bio-oil (a) and H_2 yield (b), for Ni/LaAl catalyst. 700 ºC; 0.3 $g_{catalyst}h/g_{bio\text{-}oil}$; S/C ratio = 6.

Figure 5. Effect of O/C ratio on the evolution with time on stream of the yield of CO_2 (a), CO (b), CH_4 (c) and hydrocarbons (d), for Ni/LaAl catalyst. 700 ºC; 0.3 $g_{catalyst}h/g_{bio\text{-}oil}$; S/C ratio = 6.

Figure 6. Effect of O/C ratio on the TPO profiles (a) and content coke (b) for the Ni/LaAl catalyst deactivated under the conditions in Figures 4 and 5.

Figure 7. XRD diffractograms of Ni/LaAl catalyst deactivated for different O/C ratios. 700 ºC; 0.30 $g_{catalyst}h/g_{bio\text{-}oil}$; S/C ratio = 6.

Figure 8. Effect of O/C ratio on the evolution with time on stream of bio-oil (a) and H_2 yield (b), for Rh/ZDC catalyst. 700 ºC; 0.15 $g_{catalyst}h/g_{bio\text{-}oil}$; S/C ratio = 6.

Figure 9. Effect of O/C ratio on the evolution with time on stream of the yield of CO_2 (a), CO (b), CH_4 (c) and hydrocarbons (d), for Rh/ZDC catalyst. 700 ºC; 0.15 $g_{catalyst}h/g_{bio\text{-}oil}$; S/C ratio = 6.

Figure 10. Effect of O/C ratio on the TPO profiles (a) and content coke (b) for the Rh/ZDC catalyst deactivated under the conditions in Figures 8 and 9.

Figure 11. TPR profiles of Rh/ZDC catalyst deactivated for different O/C ratios. 700 ºC; 0.15 $g_{catalyst}h/g_{bio\text{-}oil}$; S/C ratio = 6.

Figure 12. Evolution with time on stream of bio-oil conversion and product yields for the Rh/ZDC catalyst. 700 ºC; 0.6 $g_{catalyst}h/g_{bio\text{-}oil}$; S/C ratio = 6; O/C ratio = 0.34.

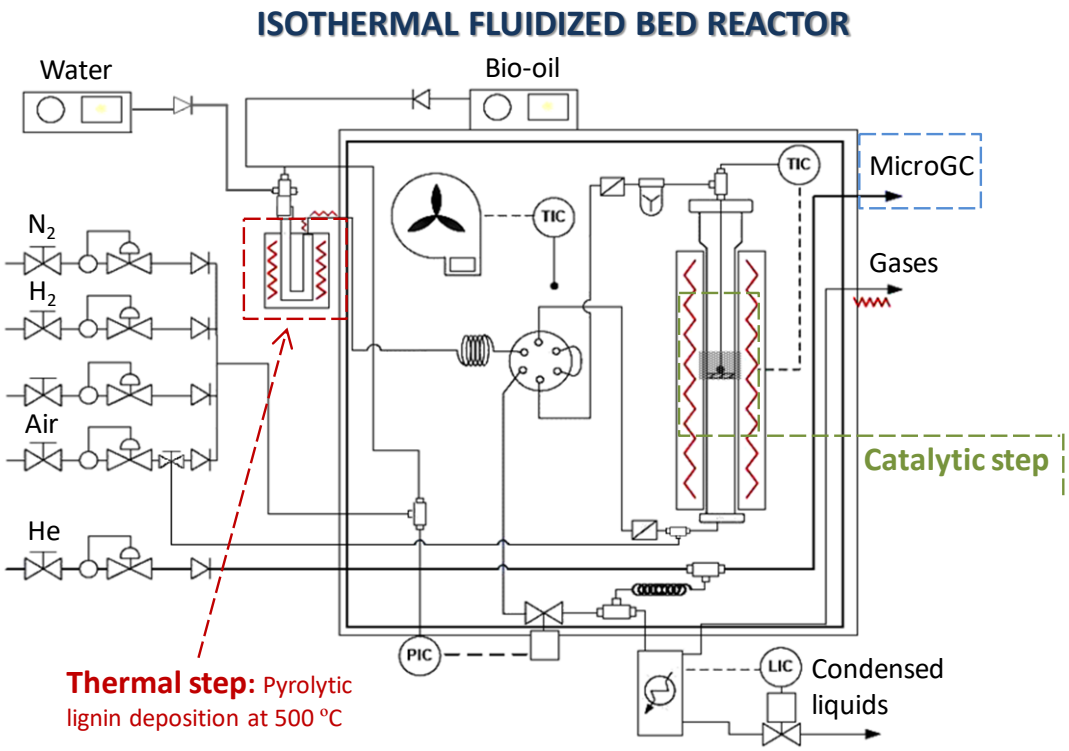
ISOTHERMAL FLUIDIZED BED REACTOR
Water
Bio-oil
MicroGC
Gases
N_2
H_2
Air
He
Catalytic step
TIC
TIC
TIC
PIC
LIC
Condensed liquids
Thermal step: Pyrolytic lignin deposition at 500 °C

Figure 1

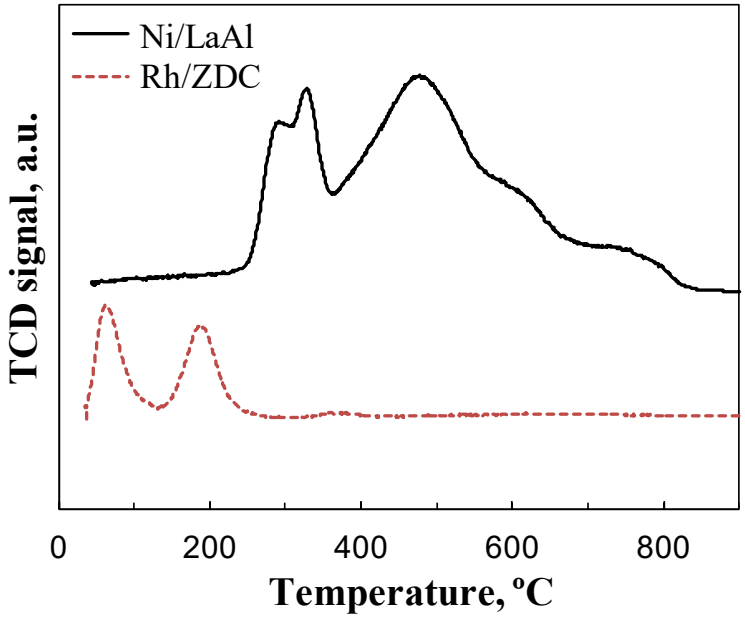

Figure 2

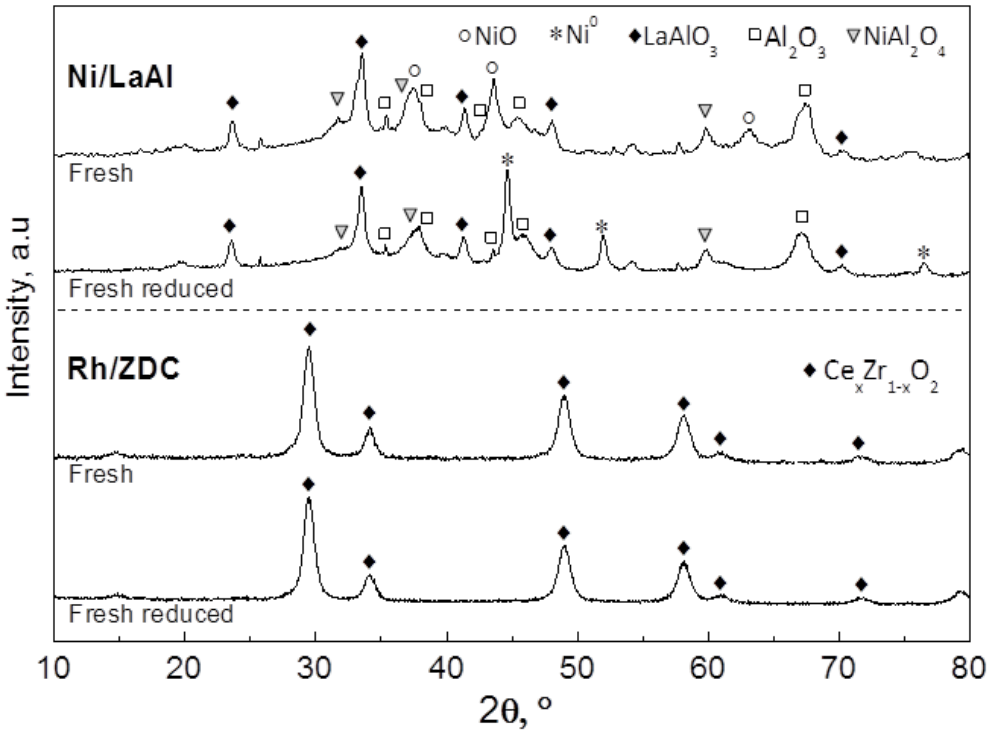
NiO
Ni0
LaAlO3
Al2O3
NiAl2O4
Ni/LaAl
Fresh
Fresh reduced
Rh/ZDC
CexZr1-xO2
Fresh
Fresh reduced
Intensity, a.u
10
20
30
40
50
60
70
80
2θ, °

Figure 3

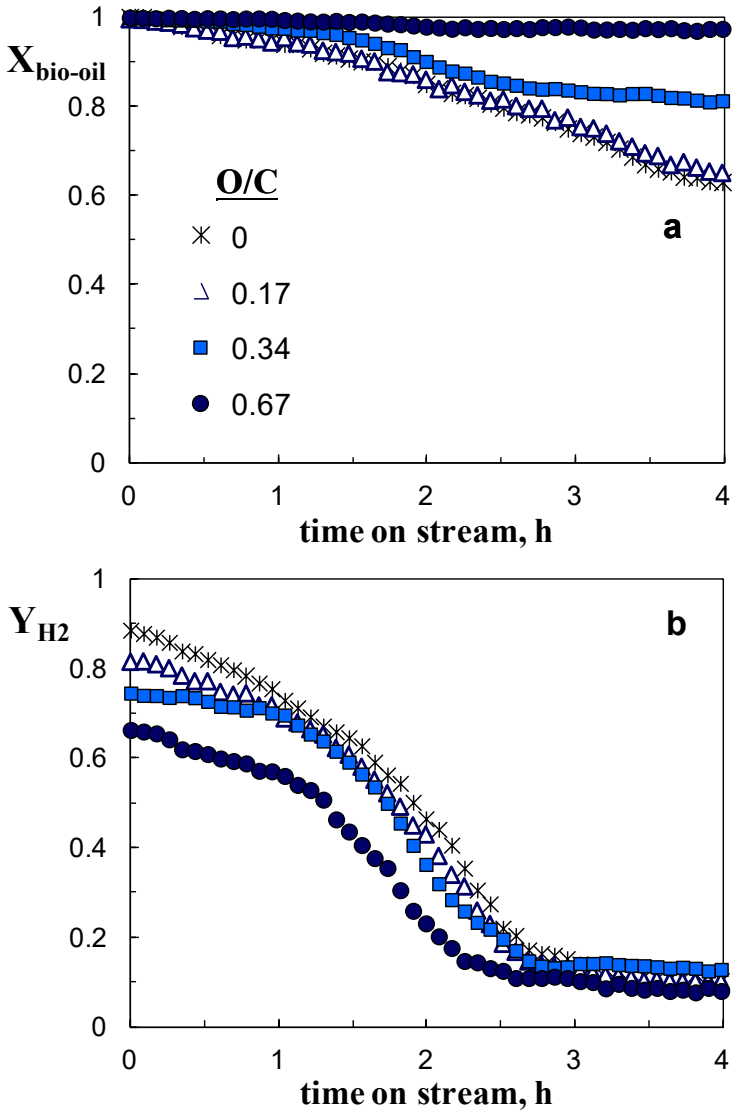
X bio-oil
1
0.8
0.6
0.4
0.2
0
O/C
0
0.17
0.34
0.67
a
0
1
2
3
4
time on stream, h
Y H2
b
time on stream, h

Figure 4

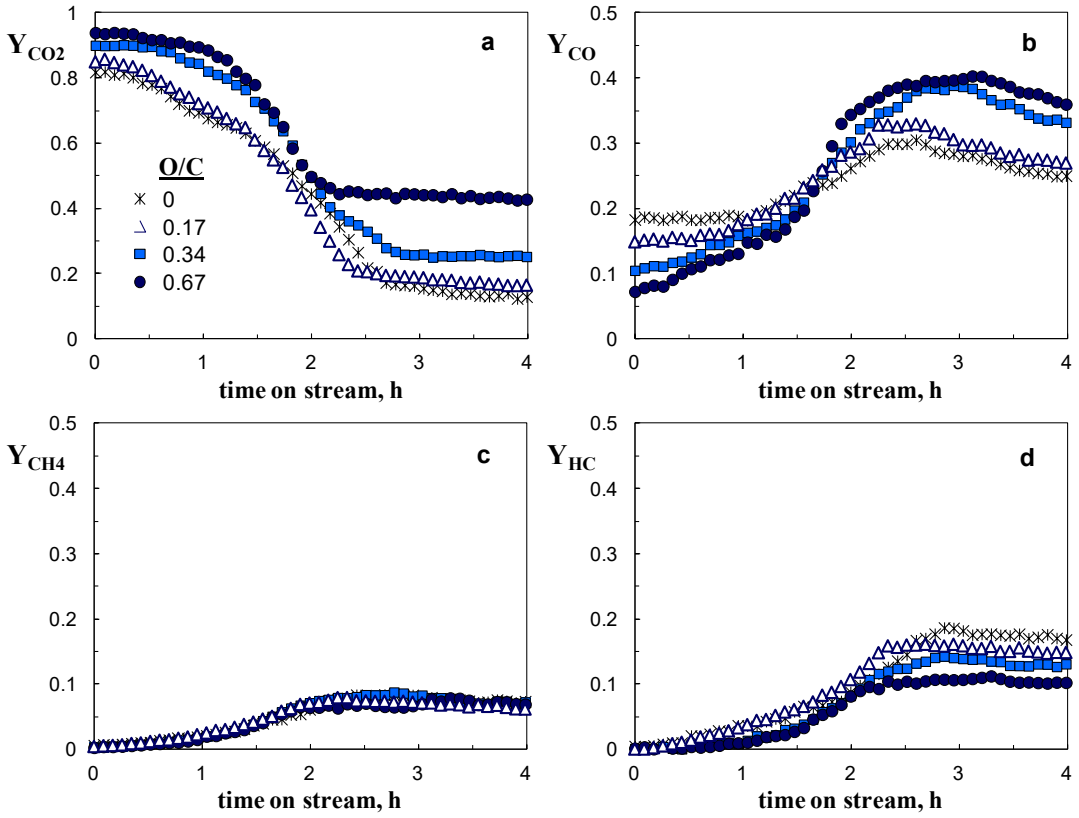
a
Y_{CO2}
O/C
0
0.17
0.34
0.67
time on stream, h
b
Y_{CO}
time on stream, h
c
Y_{CH4}
time on stream, h
d
Y_{HC}
time on stream, h

Figure 5

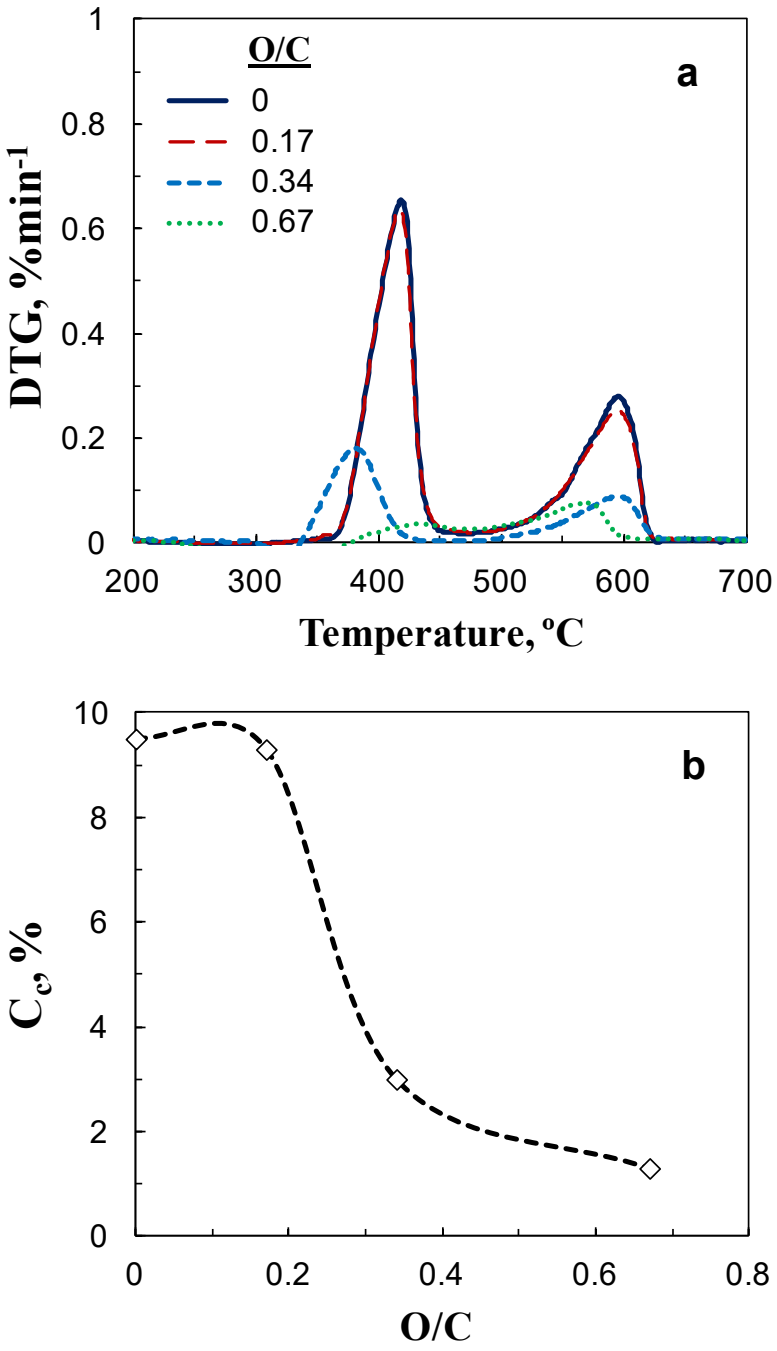

Figure 6

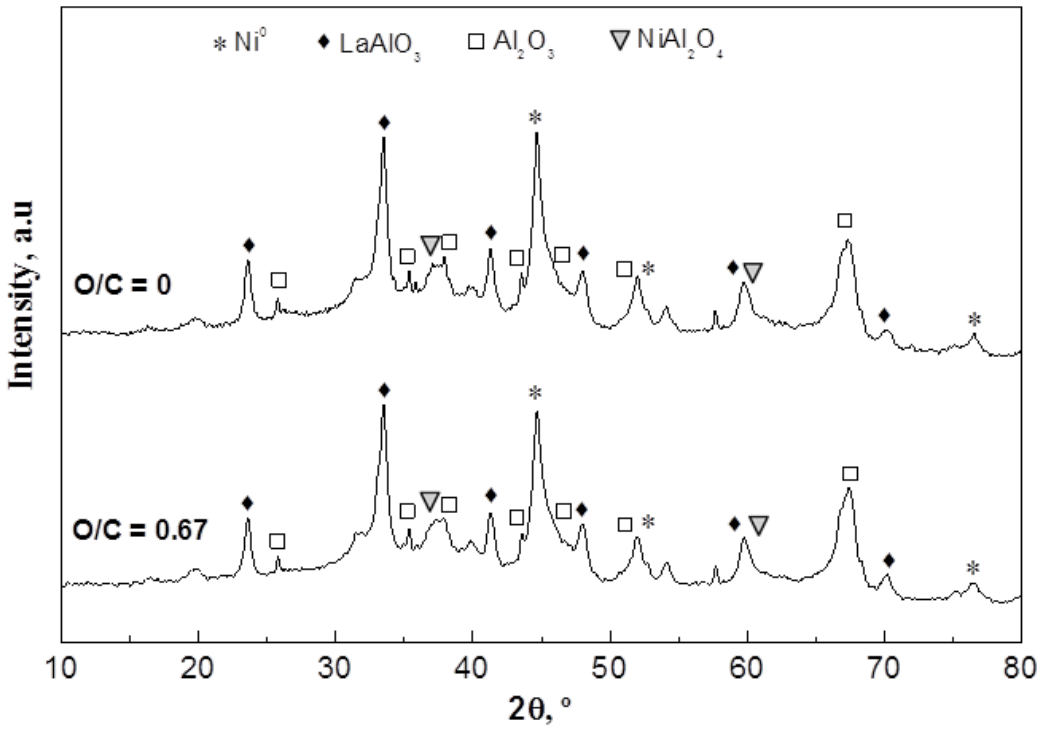
* Ni°
♦ LaAlO3
□ Al2O3
▽ NiAl2O4
O/C = 0
O/C = 0.67
Intensity, a.u
10
20
30
40
50
60
70
80
2θ, °

Figure 7

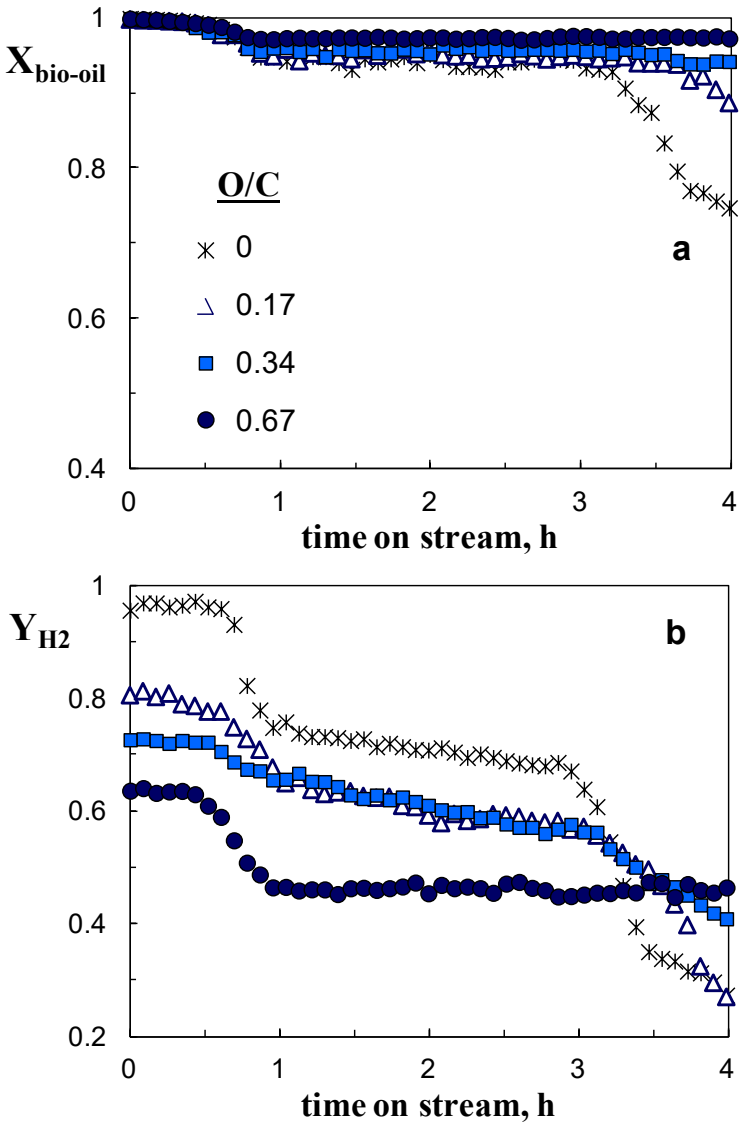
X bio-oil
1
0.8
0.6
0.4
O/C
0
0.17
0.34
0.67
a
0
1
2
3
4
time on stream, h
Y H2
b
0.2
time on stream, h

Figure 8

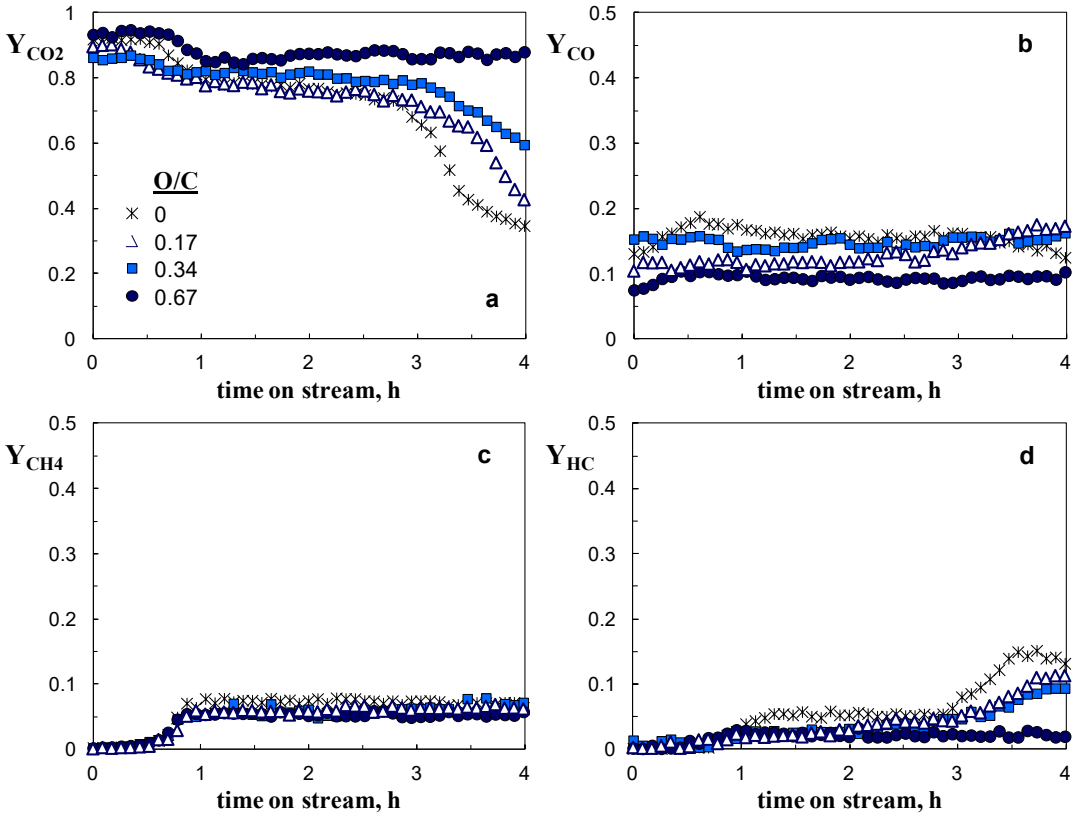
Y CO2
O/C
0
0.17
0.34
0.67
a
time on stream, h
Y CO
b
time on stream, h
Y CH4
c
time on stream, h
Y HC
d
time on stream, h

Figure 9

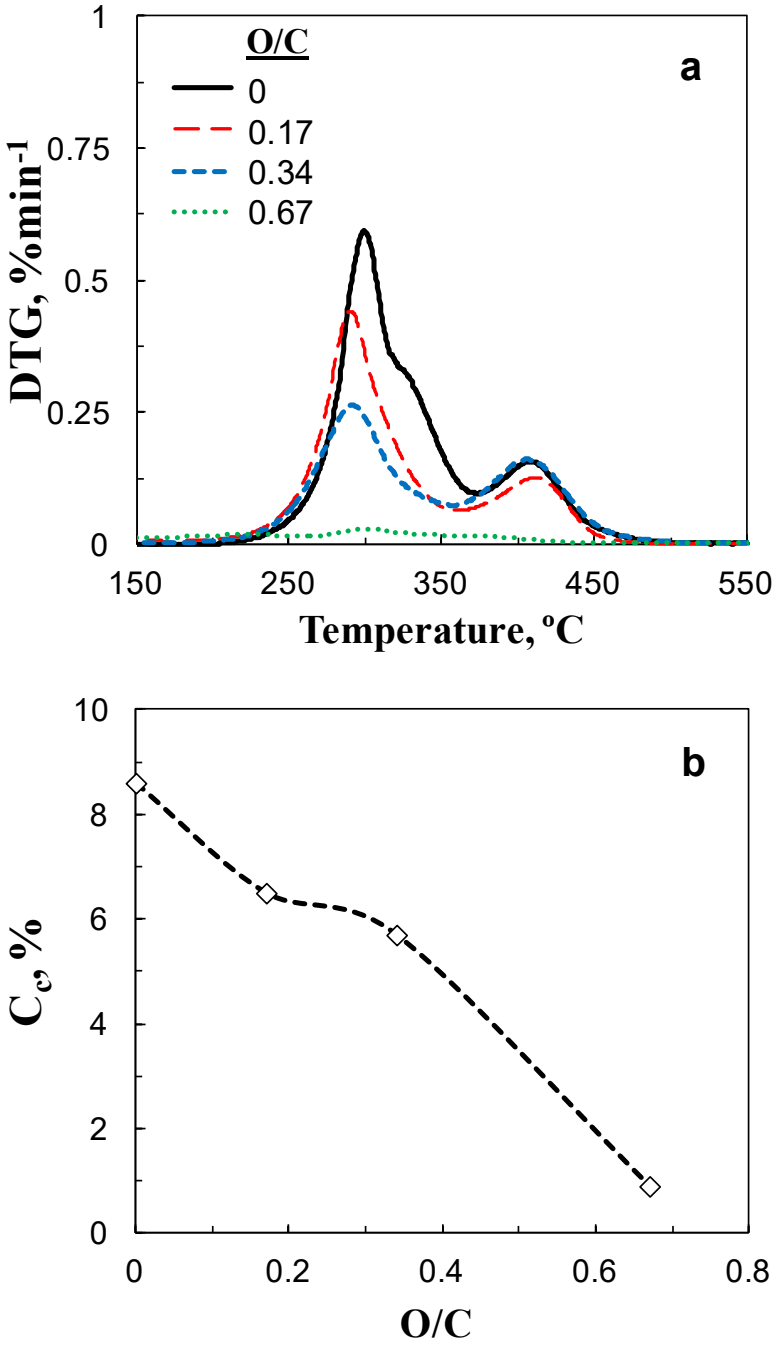

Figure 10

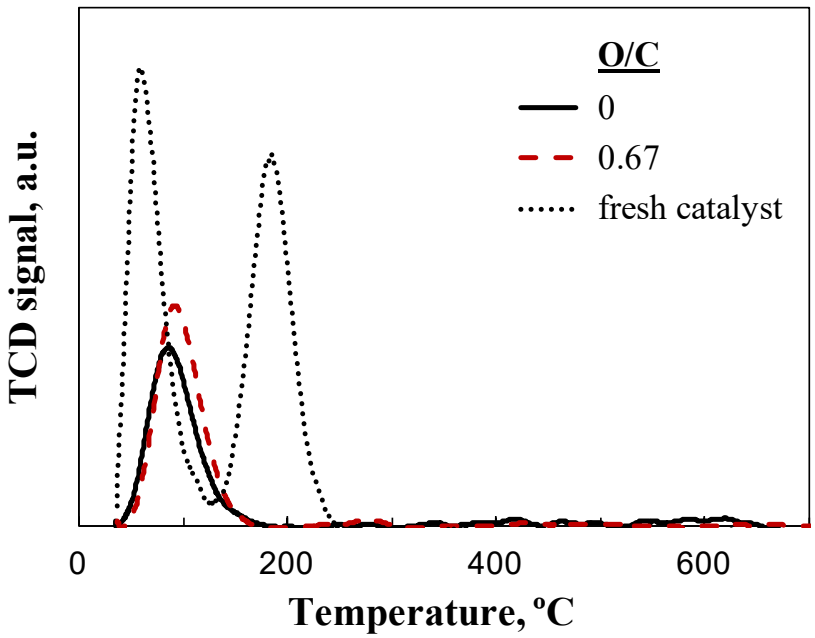
O/C
0
0.67
fresh catalyst
TCD signal, a.u.
0
200
400
600
Temperature, ºC

Figure 11

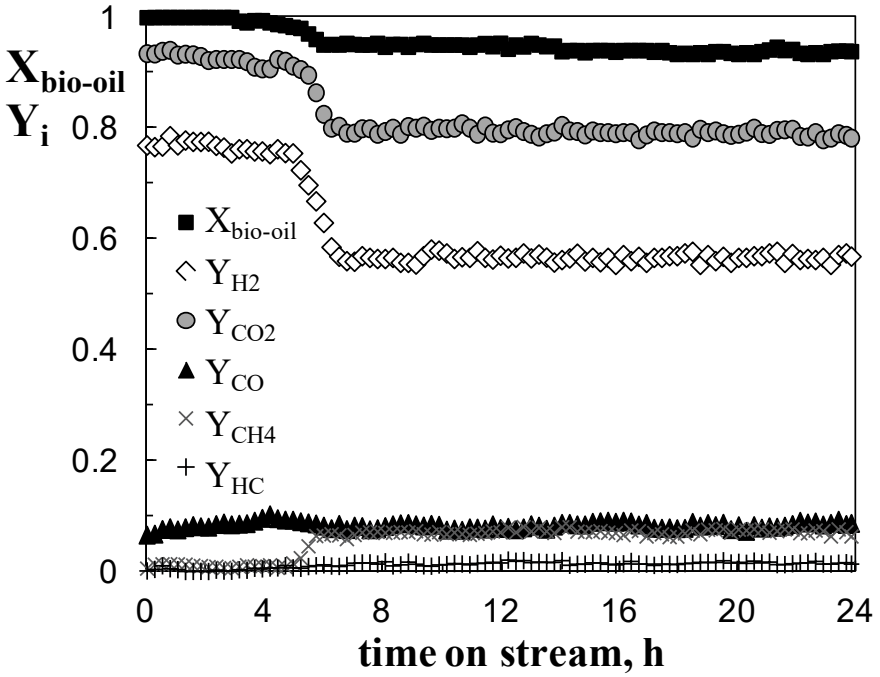
1
0.8
0.6
0.4
0.2
0
X bio-oil
Y i
X bio-oil
Y H2
Y CO2
Y CO
Y CH4
Y HC
0
4
8
12
16
20
24
time on stream, h

Figure 12

Table 1. Bio-oil physical and chemical properties.

Physical properties	
Water content (wt %)	38
pH	2.0
Density (g/ml) 25 ºC	1.107
Density (g/ml) 40 ºC	1.098
Viscosity(cP) 40 ºC	11.2
Suspended solids (wt %)	0.5
Elemental analysis on a dry basis, wt %	
C	50.5
H	7.1
N	-
O	42.4
S	-
Empiric formula (dry basis)	$C_{4.21}H_{7.14}O_{2.65}$
Ash (wt %)	< 0.1
HHV (MJ/kg)	23.5

Table 2. Bio-oil composition measured by GC-MS.

Compound or group	wt %
Acetic acid	25.25
Acetone	1.11
1-hydroxi-2-propanone	15.53
Ethanol	0.16
Hydroxiacetaldehyde	4.53
Levoglucosane	14.61
Other Ketones	6.04
Other Ácids	8.41
Esthers	3.9
Other Aldehydes	3.66
Fenols	11.54
Other Alcohols	1.01
Others	1.53
Non identified	2.72
Total	**100**

Table 3. Properties of the catalysts.

Catalyst	S_{BET} ($m^2\ g^{-1}$)	V_p ($cm^3\ g^{-1}$)	d_p (nm)	Dispersion (%)	S_m ($m^2\ g_{metal}^{-1}$)
Ni/LaAl	37.6	0.14	14.6	5.9	40
Rh/ZDC	85.7	0.31	17.7	72.4	319